

Electrochemical Detection of Hydrazine Based on Facial Synthesized Sulfur-Poly(Pyrrole-Co-Aniline) Nano-Fiber

Hui Peng^{1,*} and Chunyan Liang²

¹ School of Materials Science and Engineering, Beijing Institute of Technology, Beijing, 100081, People's Republic of China

² College of Computer Science and Technology, Shandong University of Technology, Shandong Zibo, 255049, People's Republic of China

*E-mail: cyl_bit@yahoo.com

Received: 15 July 2016 / Accepted: 18 August 2016 / Published: 6 September 2016

Chemical oxidation method was explored to prepare the poly(pyrrole-co-aniline) (PPyA) copolymer. Cetyltrimethyl ammonium chloride (CTAC) was used as the template in the oxidation reaction. Then the S/PPyA composite (nano-sulfur/poly(pyrrole-co-aniline)) was obtained by treating the mixture of sublimed sulfur and PPyA at 160 °C for 24 h. The as-prepared PPyA and S/PPyA were characterized by various techniques including X-ray powder diffraction (XRD), scanning electron microscopy (SEM), Raman spectroscopy and Fourier transform infrared spectroscopy (FTIR). The S/PPyA was used to modify the glassy carbon electrode (GCE) and the electrochemical activity of as-synthesized S/PPyA/GCE for the oxidation of hydrazine was investigated. The low detection limit of 0.18 μM (S/N=3) and fast response time within 3 s were achieved. The remarkable performance makes S/PPyA/GCE a promising electrode applied in the construction of sensors for the determination of hydrazine.

Keywords: Poly(pyrrole-co-aniline); Sensor; Electrochemistry; Hydrazine; Composite

1. INTRODUCTION

Hydrazine, regarded as major industrial commodities, can be widely used as rocket propellants, plant-growth regulators, explosives, antioxidants and corrosion inhibitor [1, 2]. Hydrazine is highly toxic and dangerous that will cause damages to brain, liver, nerve and so on [3]. Owing to the importance of hydrazine in industrial application and pharmacology, developing a rapid, sensitive and selective determination method for hydrazine is highly demanded and has received much attention from scientists [4-7].

Up to now, a large number of methods such as spectrophotometry and chemiluminescence have been reported for the detection of hydrazine. Among all reported methods, voltammetric method has a great deal of advantages such as high sensitivity and selectivity, simple operation and rapid response [8-15]. Unfortunately, large over potential was required for the oxidation reaction of hydrazine at conventional electrodes. Thus, the electrodes were modified with various organic or inorganic materials in order to decrease the over potential and improve the electron transfer rate [16-20]. Among the reported materials, electroactive polymer has shown the best advantageous characteristic and the modified electrode demonstrated outstanding sensitivity and selectivity for hydrazine determination. In Koçak's group, a gold nanoparticle modified bromocresol purple/carbon nanotube electrode was successfully prepared through the following two steps: firstly the bromocresol purple monomer was polymerized at the exterior of carbon nanotube modified GCE, and then Au nanoparticles were doped in the electrode by electrochemical reduction from their acidic solutions. Afterwards, the electrochemical behaviour of the prepared electrode for hydrazine oxidation was investigated [21]. As revealed by Aitout et al., the poly-*ortho*-methoxy-aniline was suitable for the modification of a non-conducting substrate Plexiglas which was firstly modified with Au by cementation [22]. The resulted material had demonstrated excellent activity for the oxidation reaction of hydrazine in acid aqueous solution. Owing to the rapid mass transport resulted from the large porosity, the Pd nanoparticles modified poly(*o*-phenylenediamine) colloids prepared by Liao et al. have shown excellent activity toward the hydrazine oxidation reaction [23]. A thin film of poly(4,5-dihydroxy-1,3-benzenedisulfonic acid) was prepared on the surface of multiwall carbon nanotubes modified GCE by electrochemical method in Ensafi's group [24]. Then varieties of electrochemical methods including linear sweep voltammetry, chronoamperometry and cyclic voltammetry were explored to review the electrocatalytic activity of the modified electrode for the hydrazine oxidation reaction.

In our study, a copolymer PPyA was synthesized by the copolymerization reaction between pyrrole (Py) and aniline (An) that is more available and cost less than Py. The prepared copolymer PPyA successfully embodies the merits of the two components. A novel electrochemical sensor was constructed with the PPyA modified glassy carbon electrode. And the high performance of the sensor for the oxidation of hydrazine was ensured owing to the existence of effective electrochemical reaction sites.

2. EXPERIMENTS

2.1 Preparation of PPyA nanofiber networks

A typical polymerization reaction was used to prepare the PPyA nanofibers. Certain surfactant CTAC as the template was dissolved in 200 mL of 0.1 M HCl, then Py and An monomers with the molar ratio of 1:1 were added in order and the mixture was stirred for 15 min to obtain a homogeneous solution. Subsequently, 0.6 M ammonium persulfate (APS) in 200 mL of 0.1 M HCl was added into the solution to turn on the polymerization. The molar ratio of Py/ An to APS was 1:1.

The polymerization was conducted at $-5\text{ }^{\circ}\text{C}$ for 24 h. Then the product was separated by filtration and washed with plenty of deionized ethanol and water, and then kept at $60\text{ }^{\circ}\text{C}$ under vacuum for 24 h.

2.2 Preparation of S/PPyA composite

The S/PPyA composites with different weight ratio of PPyA and sulfur (1:2, 1:3, 1:5) were prepared. The sulfur and PPyA were mixed and heated to $160\text{ }^{\circ}\text{C}$ under Ar protection for 24 h to obtain the composite. The temperature was obliged to be higher than the melting point of elemental sulfur to guarantee the effective infiltration of melting sulfur into the pores of PPyA.

2.3 Characterization

The structure of the prepared sample was characterized by X-ray diffraction (XRD, D8-Advanced, Bruker, Germany). Cu $K\alpha$ radiation was used and the range of scanning angle was from 5° to 80° . The morphology feature of the sample was measured by SEM (JSM-6510LV, Rigaku, Japan). Fourier transform infrared spectroscopy (FTIR, Nicolet iS5, Thermo Scientific, USA) and Raman spectroscopy (Renishaw, inVia) were explored to investigate the surface functional groups of the samples.

2.4 Electrochemical measurement

A glassy carbon electrode (GCE) was polished by 0.3 and $0.05\text{ }\mu\text{m}$ alumina slurry in order, and entirely washed with water and ethanol. Then, $5\text{ }\mu\text{L}$ of S/PPyA dispersion (0.5 mg/mL) was added onto the surface of GCE and dried in air room temperature.

The electrochemical tests were conducted on the CHI430a electrochemical workstation (USA) with a conventional three electrode system including a working electrode (modified GCE), auxiliary electrode (platinum wire) and a reference electrode (Ag/AgCl). All experiments were studied at room temperature. Electrochemical impedance spectroscopy (EIS) and cyclic voltammetry (CV) was used for characterizing the electrode resistance performance. 5 mM $[\text{Fe}(\text{CN})_6]^{3-/4-}$ was used as probe, 0.1 M KCl was used as supporting electrolyte. Frequency range was set as 10^1 to 10^5 Hz and the amplitude was set as 10 mV .

3. RESULTS AND DISCUSSION

The morphology feature of PPyA and S/PPyA was measured by SEM and the results were presented in Fig. 1. The morphology property of nanofiber network of PPyA was obtained using CTAC as the template. When the concentration of CTAC was kept at a certain value, cylindrical micelles of CTAC could be formed. The preparation of 1D structures was dependent on the yield of $(\text{CTA})_2\text{S}_2\text{O}_8$ [25]. Then the micellar 3D networks were formed by the aggregation of CTAC micelles

with monomers. PPyA with interconnected nanofiber network was synthesized using the soft template that could direct the synthetic track. The as-synthesized nanofibers were highly uniform and the size distribution was in a narrow diameter of about 80 nm. The pores between the nanofibers could be clearly observed. In the preparation process of S/PPyA, some parameters were chosen as follows: heating temperature as 160 °C that is slightly higher than the melting point of elemental sulfur in order to obtain low viscosity, and treating time as 24 h for the sake of distributing sulfur into the pores of network structure and contacting with PPyA nanofibers fully. The morphology feature of nanofiber network of the obtained S/PPyA changed distinctly compared with that of PPyA. As can be seen from the SEM image of S/PPyA composite, the nanofibers was closer to each other and the diameter changed from 80 nm to 110 nm. The pore channels between nanofibers became smaller owing to the addition of elemental sulfur.

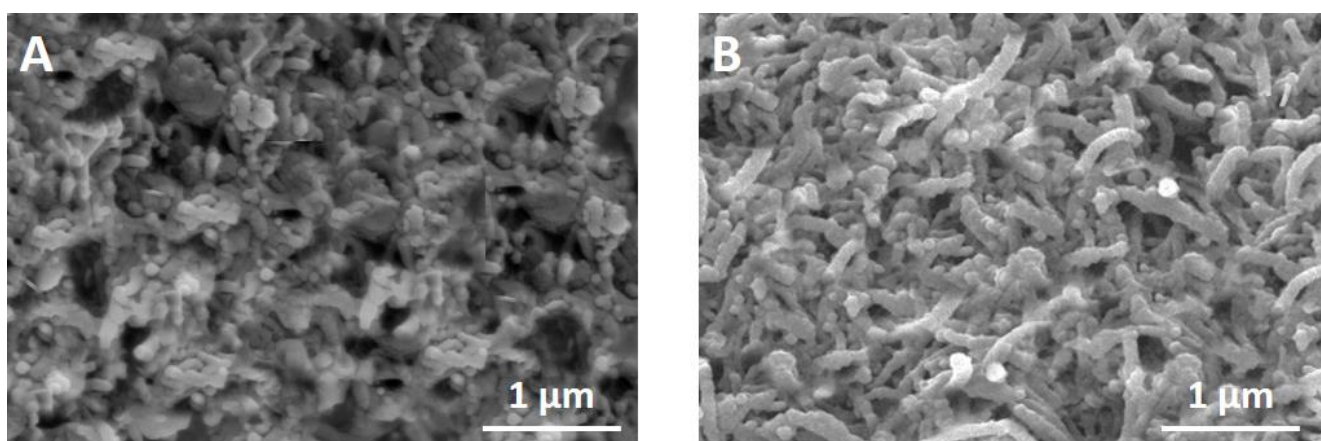


Figure 1. SEM images of (A) PPyA and (B) S/PPyA.

The XRD patterns of PPyA and S/PPyA are shown in Fig. 2A. As shown in the XRD pattern of PPyA, a broad peak at $2\theta = 22.6^\circ$ was observed which suggesting the amorphous structure of PPyA. For the S/PPyA composite, both a board peak around 20° related to PPyA and many other peaks resulted from the elemental sulphur with Fddd orthorhombic structure [26] were observed. The result demonstrated that only a fraction of nano-sulphur was achieved and dispersed uniformly in the network structure of PPyA ploymer. Nevertheless, during the cooling process, a crystal structure was formed by the large amount of rest sulphur because of the limited space.

Raman spectra of PPyA and S/PPyA composite were measured using 514.5 nm diode laser excitation and the results were shown in Fig. 2B. The peaks under 500 cm^{-1} belong to the sulphur element [27] and another two peaks at 1597 and 1355 cm^{-1} are related to C–C and C–N groups respectively. Therefore, the composite S/PPyA composed of both sulphur and PPyA was successfully prepared in our work.

The functional groups in the PAN, PPy, PPyA and S/PPyA composite was characterized by FTIR (Fig. 3). As to PAN, the characteristic peaks at 1142 , 1242 , 1300 , 1491 and 1567 cm^{-1} are ascribed to C=N, C–N⁺, C–N, C=C stretching deformation of benzenoid rings and quinoid,

respectively. For PPy, the peaks at 1045, 1126, 1485 and 1549 cm^{-1} represented C–H in plane bending, C–N stretching, C=N stretching and C=C stretching, respectively [28, 29].

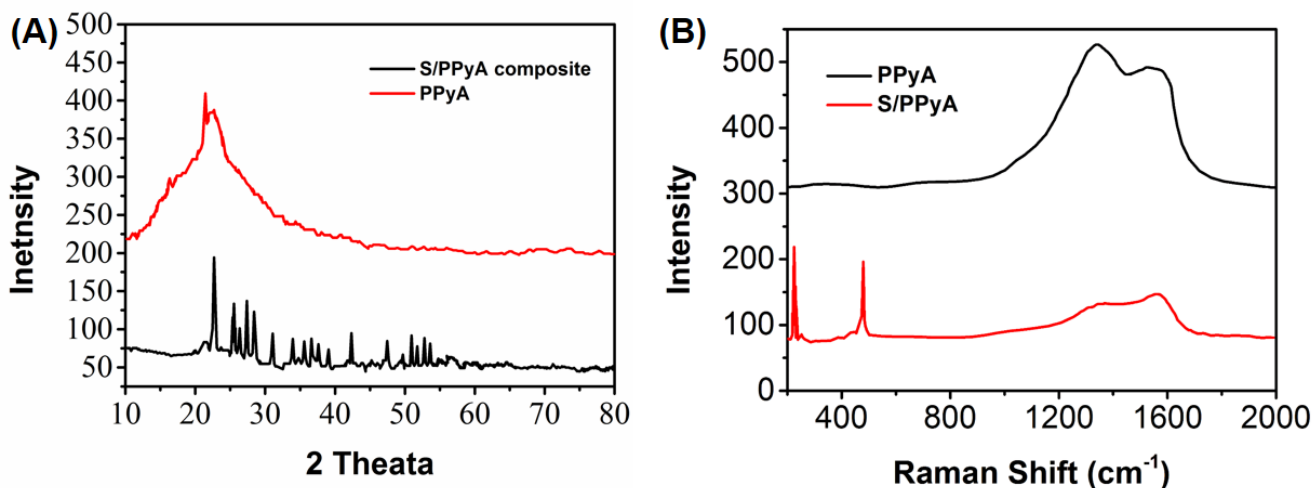


Figure 2. (A) XRD patterns of PPyA and S/PPyA composite. (B) Raman spectra of PPyA and S/PPyA composite.

As can be seen from the FTIR spectrum of PPyA, the peaks at 1146, 1309, 1490, 1570 cm^{-1} that are resulted from the vibration of both pyrrole rings and PAn could be observed, indicating the successful preparation of the copolymer PPyA. The peak at 1299 cm^{-1} was the characteristic peak of aromatic NH groups [30, 31].

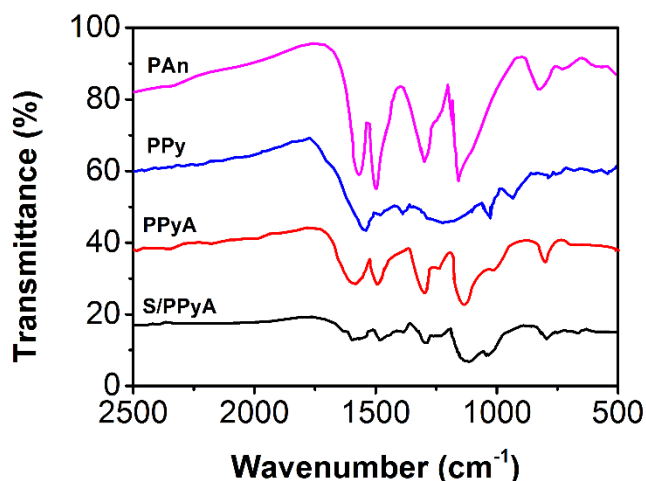


Figure 3. FTIR spectrum of PAn, PPy, PPyA and S/PPyA composite.

The surface status of the modified electrode can be evaluated conveniently and effectively by cyclic voltammograms (CVs) of ferricyanide owing to the importance of the barrier or defects in the electron transfer process between the electrode and the reaction substance [32]. Therefore, the changes of the electrode behaviour after modification were investigated using cyclic voltammograms (CVs) of ferricyanide as a probe. On the other hand, the electron transfer kinetics of $[\text{Fe}(\text{CN})_6]^{3-/4-}$ could be

deduced. The cyclic voltammograms of bare GCE, PPyA/GCE and S/PPyA/GCE recorded in a 5 mM $[\text{Fe}(\text{CN})_6]^{3-/4-}$ solution containing 0.1 M KCl at a scan rate of 100 mV/s were shown in Fig. 4A. The well-defined reduction and oxidation peaks resulted from the $\text{Fe}^{3+}/\text{Fe}^{2+}$ redox couple could be obviously observed on the tested three electrodes. Due to the poor electroconductivity of PPyA layer formed on the surface of GCE, the peak current obtained on PPyA/GCE was lower than that obtained on the bare GCE. However, the S/PPyA/GCE exhibited the highest peak current due to the addition of sulphur that owns the highest electrocatalytic activity. Furthermore, compared with that obtained on GCE and PPyA/GCE, the interval of peak-to-peak potential obtained on S/PPyA/GCE was smaller. EIS technique was also explored to evaluate the performance of three electrodes and the experiments were carried out as follows: 5 mM $[\text{Fe}(\text{CN})_6]^{3-/4-}$ as the probe, frequency ranging from 10 kHz to 0.1 Hz and AC amplitude of 10 mV. The Nyquist plots obtained were shown in Fig. 4B. The semicircular portion occurred at higher frequency is related to the electron transfer-limited process, and the diameter of semicircle corresponds to the electron transfer resistance (R_{et}). The electron transfer resistance of S/PPyA/GCE was lower than that of bare GCE and PPyA/GCE, indicating the electron transfer is faster on S/PPyA/GCE.

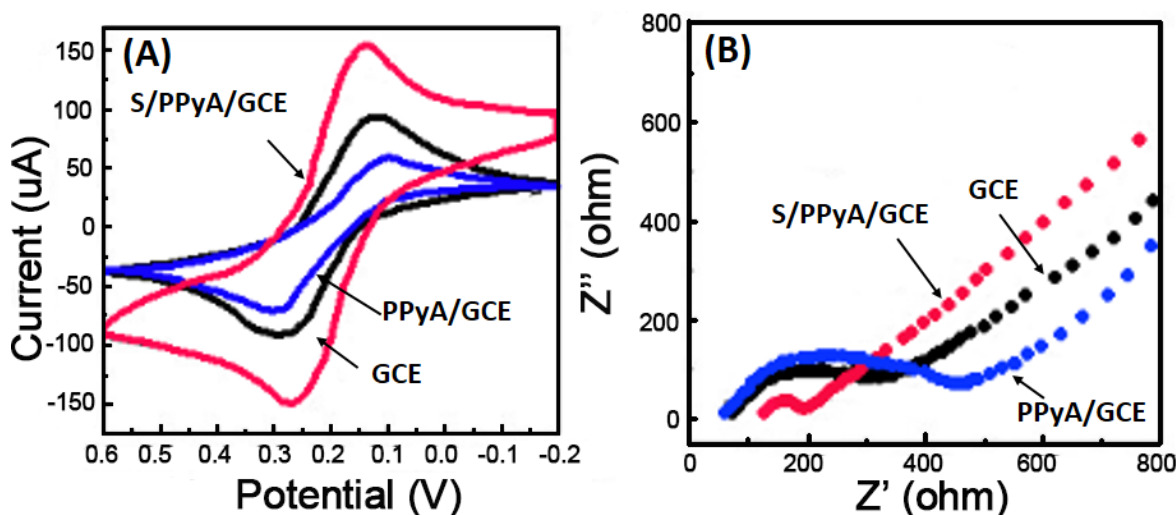


Figure 4. (A) CVs of bare GCE, PPyA/GCE and S/PPyA/GCE in 5 mM $[\text{Fe}(\text{CN})_6]^{3-/4-}$ solution containing 0.1 M KCl at a scan rate of 100 mV/s. (B) Nyquist plots of 5 mM $[\text{Fe}(\text{CN})_6]^{3-/4-}$ in 0.1 M KCl from 10 kHz to 0.1 Hz at an ac amplitude of 10 mV under open-circuit potential conditions obtained for bare GCE, PPyA/GCE and S/PPyA/GCE.

The electrocatalytic behavior of S/PPyA/GCE towards hydrazine oxidation (0.2 mM) was investigated using CV technique and the results were compared with that of bare GCE. As shown in Fig. 5, no anodic peak was observed on bare GCE, indicating the nonoccurrence of hydrazine oxidation. Nevertheless, in the CVs obtained on S/PPyA/GCE, an outstanding oxidation current with the distinct peak at 0.12 V was appeared. The peak current was approximately 29.7 times higher than that obtained on the bare GCE, which could be resulted from the reversibility of the electron transfer process and the accumulation of the electrochemical active species on the high surface area of

electrode. The determination method for hydrazine using electrocatalytic oxidation at low potential (0.12 V) is highly promising for industrial applications owing to the avoid of interference.

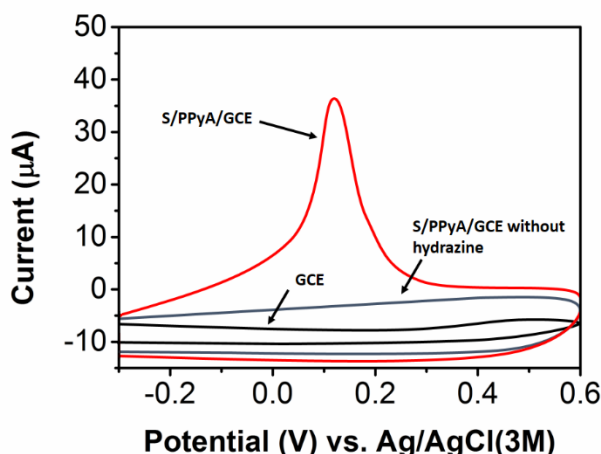


Figure 5. CVs of 0.2 mM hydrazine in 0.1 M PBS on the bare GCE and S/PPyA/GCE. Scan rate: 50 mV/s.

The electrochemical behaviour of hydrazine depends on the pH value of PBS. As shown in Fig. 6A, when the pH increased from 4.0 to 7.0, the peak current increased. However, when pH increased from 7.0 to 9.0, the peak current remained nearly constant. The peak current was small at low pH, which was resulted from the formed inactive protonated hydrazine under low pH since the pK_a of hydrazine is 7.9. After comprehensive consideration, PBS solution with pH of 7.4 was selected.

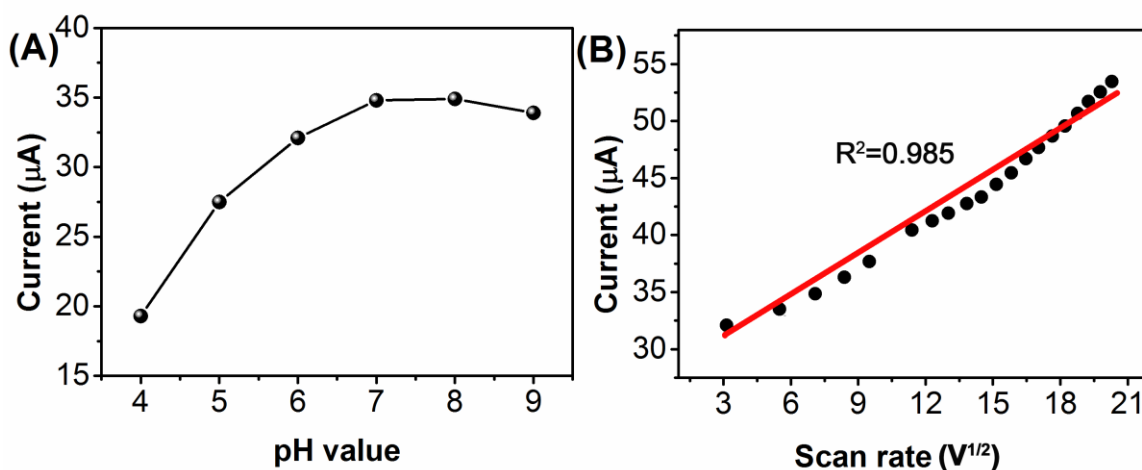


Figure 6. Effect of (A) pH value and (B) scan rate of hydrazine detection using S/PPyA/GCE.

The influence of scan rate on the oxidation of hydrazine on S/PPyA/GCE was also investigated by CV (Fig. 6B). The anodic peak current was related linearly with the square root of scan rate ($v^{1/2}$) when it ranging from 10-400 mV/s. Moreover, as shown in Fig. 7, when the immersed time increased,

the peak current did not increase, demonstrating the electron transfer process was diffusion-controlled in the oxidation of hydrazine on S/PPyA/GCE.

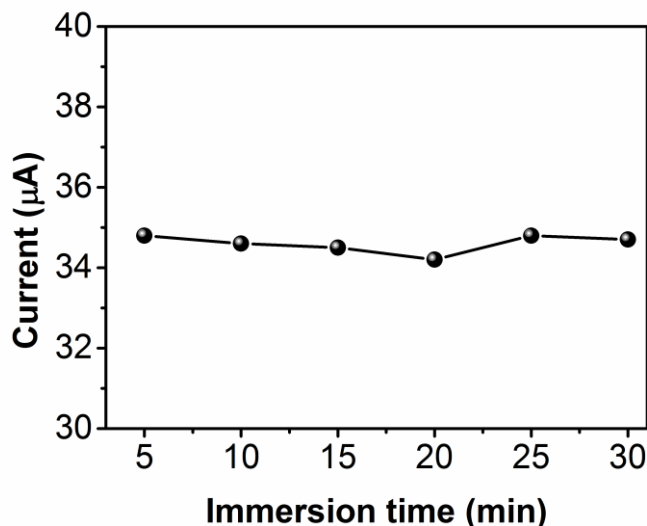
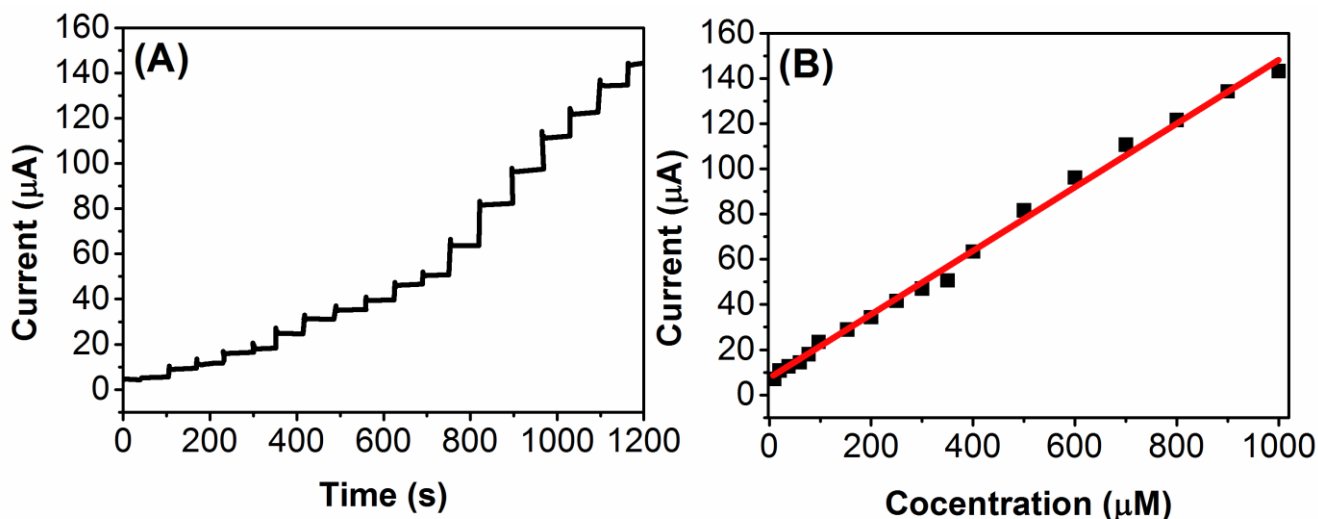


Figure 7. Effect of immersion time of hydrazine detection using S/PPyA/GCE.



b

Figure 8. (A) Typical steady-state response of the S/PPyA/GCE to successive injection of hydrazine into the stirred 0.1 M PBS at pH 7.0. (B) The calibration curve (applied potential: 0.12 V).

According to the cyclic voltammetric results described above, the detection limit for hydrazine determination on S/PPyA/GCE was measured by amperometric current-time response. The hydrazine amperogram recorded during the addition of hydrazine with the potential kept at +0.12 V was shown in Fig.8A. The amperometric response observed was well-defined, indicating the catalytic performance of the S/PPyA/GCE for the oxidation of hydrazine stably and efficiently. The response current was in linear correlation with the concentration of hydrazine ranging from 1 µM to 1 mM, and the correlation equation could be described as: $I_p (\mu A) = 1.332C + 3.552$ ($R = 0.998$). The detection limit calculated

with S/N=3 was 0.18 μ M. The performance of S/PPyA/GCE for the determination of hydrazine was compared with previously reported modified electrodes. As presented in Fig. 8B, the designed S/PPyA/GCE in our work demonstrated wide linear range and lower detection limit.

We tested the reliability of proposed hydrazine electrochemical sensor. The S/PPyA/GCE was used for determination of hydrazine in real agriculture waste water sample by amperometric measurement. The standard addition method was adopted for examining the recovery of hydrazine in water samples. The results of real sample determination was summarized in Table 1.

Table 1. Determination of hydrazine in agriculture wastewater samples using S/PPyA/GCE.

Sample	Added (nM)	Found (nM)	Recovery (%)	RSD (%)
Sample 1	0	0	—	0.02
Sample 2	20	16.78	95.7	1.57
Sample 3	50	50.21	101.3	0.14
Sample 4	100	100.56	102.0	1.09

4. CONCLUSIONS

A novel S/PPyA composite was synthesized by treating a mixture of sulfur and PPyA at 160 °C for 24 h. The as-synthesized S/PPyA composite was in a network structure that is in favour of electrochemical detection. The electrochemical activity of S/PPyA modified GCE toward the oxidation of hydrazine was investigated. The outstanding performance of S/PPyA/GCE (e.g., lower detection limit of 0.18 μ M, wider linear range and rapid response) demonstrates the promising potential of S/PPyA /GCE applied in the construction of effective sensors for the determination of hydrazine.

References

1. K. Yamada, K. Yasuda, N. Fujiwara, Z. Siroma, H. Tanaka, Y. Miyazaki and T. Kobayashi, *Electrochemistry communications*, 5 (2003) 892
2. S. Amlathe and V. Gupta, *The Analyst*, 113 (1988) 1481
3. S. Golabi and H. Zare, *Journal of electroanalytical Chemistry*, 465 (1999) 168
4. X. Zheng, Z. Zhang, Z. Guo and Q. Wang, *The Analyst*, 127 (2002) 1375
5. S. Chakraborty and C.R. Raj, *Sensors and Actuators B: Chemical*, 147 (2010) 222
6. J.S. Pinter, K.L. Brown, P.A. DeYoung and G.F. Peaslee, *Talanta*, 71 (2007) 1219
7. W. Siangproh, O. Chailapakul, R. Laocharoensuk and J. Wang, *Talanta*, 67 (2005) 903
8. H. Zhang, J. Huang, H. Hou and T. You, *Electroanalysis*, 21 (2009) 1869
9. L. Zheng and J.-f. Song, *Talanta*, 79 (2009) 319
10. A. Salimi, L. Miranzadeh and R. Hallaj, *Talanta*, 75 (2008) 147
11. A. Ejaz, M.S. Ahmed and S. Jeon, *Sensors and Actuators B: Chemical*, 221 (2015) 1256
12. Ç.C. Koçak, A. Altın, B. Aslışen and S. Koçak, *Int. J. Electrochem. Sc.*, 11 (2016) 233
13. B. Zhou, J. Yang and X. Jiang, *Mater. Lett.*, 159 (2015) 362

14. M. Ongaro, M. Signoreto, V. Trevisan, A.M. Stortini and P. Ugo, *Chemosensors*, 3 (2015) 146
15. A. Benvidi, S. Jahanbani, B.-F. Mirjalili and R. Zare, *Chinese Journal of Catalysis*, 37 (2016) 549
16. G. Hu, Z. Zhou, Y. Guo, H. Hou and S. Shao, *Electrochemistry Communications*, 12 (2010) 422
17. Q. Yi and W. Yu, *Journal of Electroanalytical Chemistry*, 633 (2009) 159
18. J. Zheng, Q. Sheng, L. Li and Y. Shen, *Journal of Electroanalytical Chemistry*, 611 (2007) 155
19. K.I. Ozoemena and T. Nyokong, *Talanta*, 67 (2005) 162
20. A.S. Adekunle and K.I. Ozoemena, *Journal of Electroanalytical Chemistry*, 645 (2010) 41
21. S. Koçak and B. Aslışen, *Sensors and Actuators B: Chemical*, 196 (2014) 610
22. R. Aitout, A. Belgaid, L. Makhoulfi and B. Saidani, *Reactive and Functional Polymers*, 66 (2006) 373
23. F. Liao, Z. Wang, T. Guo, T. Zhang and Z. Wu, *Journal of Electroanalytical Chemistry*, 673 (2012) 38
24. A.A. Ensafi and M. Lotfi, *Journal of Analytical Chemistry*, 69 (2014) 548
25. W. Zhong, S. Liu, X. Chen, Y. Wang and W. Yang, *Macromolecules*, 39 (2006) 3224
26. J.-W. Choi, J.-K. Kim, G. Cheruvally, J.-H. Ahn, H.-J. Ahn and K.-W. Kim, *Electrochimica Acta*, 52 (2007) 2075
27. J.D. Pasteris, J.J. Freeman, S.K. Goffredi and K.R. Buck, *Chemical Geology*, 180 (2001) 3
28. X.-R. Zeng and T.-M. Ko, *Polymer*, 39 (1998) 1187
29. K. Cheah, M. Forsyth and V.-T. Truong, *Synthetic metals*, 94 (1998) 215
30. G.S. Akundy, R. Rajagopalan and J.O. Iroh, *Journal of applied polymer science*, 83 (2002) 1970
31. R. Rajagopalan and J.O. Iroh, *Appl. Surf. Sci.*, 218 (2003) 58
32. A.A. Karyakin, E.E. Karyakina and H.L. Schmidt, *Electroanalysis*, 11 (1999) 149